P H Y S I C A L   R E V I E W   L E T T E R S

Effect of a Single Localized Impurity on the Local Density of States in Monolayer and Bilayer Graphene

Cristina Bena

Service de Physique Théorique, CEA/Saclay, Orme des Merisiers, 91190 Gif-sur-Yvette CEDEX, France
(Received 30 July 2007; published 20 February 2008)

We use the *T*-matrix approximation to analyze the effect of a localized impurity on the local density of states in monolayer and bilayer graphene. For monolayer graphene the Friedel oscillations generated by intranodal scattering obey an inverse-square law, while the internodal ones obey an inverse law. In the Fourier transform this translates into a filled circle of high intensity in the center of the Brillouin zone, and empty circular contours around its corners. For bilayer graphene both types of oscillations obey an inverse law.

Graphene has been studied extensively in recent years. Its most fascinating aspect is the existence of linearly dispersing gapless excitations in the vicinity of the Dirac points. This gives rise to very interesting electronic properties such as Friedel oscillations in the local density of states at low energy, which decay as $1/r^2$ [1,2] instead of the usual $1/r$ characteristic to two-dimensional systems [3,4]. It is very important to understand well the physics of impurity scattering in graphene, by studying, for example, the local density of states (LDOS) in the presence of single-impurity scattering [1–3,5]. Comparison with experiments can provide information about graphene's fundamental physics, and about the nature of the impurities.

In this Letter we analyze the Fourier transform of the density of states measurable by Fourier transform scanning tunneling spectroscopy (FTSTS). Such measurements have recently been developed for graphene [6], as well as for other two-dimensional materials such as ErSi$_2$ [7] and the cuprates [8].

Our first observation is that the FTSTS spectra can be used to distinguish between monolayer and bilayer graphene. In particular, for monolayer graphene with a localized (delta-function) impurity potential, the Friedel oscillations generated by intranodal scattering decay as $1/r^2$ at low STM bias, consistent with previous analysis [1,2]. In the FTSTS spectra this is manifested by a filled circle of high intensity in the center of the Brillouin zone (BZ), with a radius proportional to the STM bias. On the other hand, the Friedel oscillations generated by the scattering of quasiparticles between different Dirac points decay as $1/r$. In the FTSTS spectra these oscillations are translated into circular contours of high intensity centered around the corners of the BZ and around sites of the reciprocal lattice. Because of the form of the underlying Hamiltonian, the distribution of intensity on some of these circles is not rotationally invariant.

For the bilayer system, at low energy the oscillations due to both intranodal and internodal scattering have a $1/r$ dependence, corresponding to circular lines of high intensity close to center and the corners of the BZ,

and around the sites of the reciprocal lattice. At higher energies the splitting of the bands for the bilayer sample is also observable in the FTSTS spectra.

We also note that the FTSTS spectra can distinguish between different types of impurities. For example, for the case of a screened-charge impurity, the effect of internodal scattering is greatly reduced compared to the effect of intranodal scattering. This gives a clear signature in the FTSTS spectra which can be observed in an experiment.

Our last observation is that the FTSTS spectra, besides providing information about the band structure of graphene, can also give insight into the underlying Hamiltonian. In particular, the shift of the decay of the Friedel oscillations from $1/r$ to $1/r^2$, and the rotational asymmetry of some of the high-intensity spots, are strongly dependent on the peculiar form of the tight-binding Hamiltonian, and cannot be deduced solely from band-structure arguments.

The tight-binding Hamiltonian for monolayer graphene is

$$\mathcal{H} = \int d^2\vec{k} [a_{\vec{k}}^\dagger b_{\vec{k}} f(\vec{k}) + \text{H.c.}], \tag{1}$$

where the operators $a^\dagger$, $b^\dagger$ correspond to creating electrons on the sublattice A and B, respectively, and $f(\vec{k}) = -t \sum_{j=1}^3 \exp(i\vec{k} \cdot \vec{a}_j)$. Here $\vec{a}_1 = a(\sqrt{3}\hat{x} + \hat{y})/2$, $\vec{a}_2 = a(-\sqrt{3}\hat{x} + \hat{y})/2$, $\vec{a}_3 = -a\hat{y}$, t is the nearest-neighbor hopping amplitude, and a is the spacing between two adjacent carbon atoms, which we are setting to 1.

We will use this form of the Hamiltonian when performing our numerical analysis of the FTSTS spectra. However, it is useful to expand the Hamiltonian close to the corners of the BZ, which we also denote as nodes or "Dirac points," and use the linearized form to solve the problem analytically at low energies. The momenta of the six corners of the Brillouin zone are given by $\vec{K}_{1,2} = [\pm 4\pi/(3\sqrt{3}), 0]$, $\vec{K}_{3,4} = [\pm 2\pi/(3\sqrt{3}), 2\pi/3]$, $\vec{K}_{5,6} = [\pm 2\pi/(3\sqrt{3}), -2\pi/3]$. Close to each corner, m, of the BZ we can write $f(\vec{q} + \vec{K}_m) \approx \tilde{\phi}_m(\vec{q}) = v_m \vec{q} \cdot \vec{J}_m$,

where $\vec{q}$ denotes the distance from the respective corner. Also $v_{1,2} = 3t/2 = v$, $v_{3,4} = v\exp(-i\pi/3)$, $v_{5,6} = v\exp(i\pi/3)$ and $\vec{J}_{1,2} = (\pm 1, -i)$, $\vec{J}_{3,4} = \vec{J}_{5,6} = (\pm 1, i)$.

The corresponding Green's function, $\mathcal{G}(\vec{k}, \omega)$, derived from the tight-binding Hamiltonian in Eq. (1) can be expanded at low energy around the six nodes (denoted m), and in the 2×2 (A, B) sublattice basis can be written as

$$\mathcal{G}(\vec{k}, \omega) \approx G_m(\vec{k}, \omega) = \frac{1}{\omega^2 - |\tilde{\phi}_m(\vec{k})|^2} \begin{pmatrix} \omega + i\delta & \tilde{\phi}_m(\vec{k}) \\ \tilde{\phi}_m^*(\vec{k}) & \omega + i\delta \end{pmatrix}, \tag{2}$$

where δ is the quasiparticle inverse lifetime. The Fourier transform of the linearized Green's function is given by

$$G_m(\vec{r}, \omega) \propto \omega \begin{pmatrix} H_0^{(1)}(z) & i\phi_m(\vec{r})H_1^{(1)}(z) \\ i\phi_m^*(\vec{r})H_1^{(1)}(z) & H_0^{(1)}(z) \end{pmatrix}, \tag{3}$$

where $z \equiv \omega r/v$, $H_{0,1}^{(1)}(r)$ are Hankel functions, $r = |\vec{r}|$, and $\phi_m(\vec{r}) = v_m \vec{r} \cdot \vec{J}_m/(vr)$.

We first focus on a delta-function impurity localized on an atom belonging to sublattice A. In the (A, B) basis the impurity potential matrix V has only one nonzero component $V_{11} = u$. We start with a T-matrix study [3,9] of the full Hamiltonian presented in Eq. (1), and we analyze our results numerically for various energies. The resulting FTSTS spectra (corresponding to the real part of the Fourier transform of the LDOS) are plotted in Fig. 1. There are several interesting features that should be noted. First, there are regions of high intensity in the FTSTS spectra corresponding to intranodal quasiparticle scattering (central region) and internodal scattering (outer regions). Similar features have also been observed experimentally [6]. The high-intensity regions that we find are pointlike at zero energy, and acquire distinct features as one increases the energy (STM bias). Thus, at low energy the central high-intensity region is a filled circle, while the outer regions are empty. Also, the rotational symmetry of the high-intensity regions located at the corners of the BZ is broken, while it is preserved for the high-intensity regions centered on sites of the reciprocal lattice. With increasing the energy even higher, other effects such as the changing of the shape of the equal-energy contours from circular to triangular (trigonal warping) start playing an important role. At very high energy the FTSTS intensity map becomes quite intricate.

We now turn to the analytical study of the dependence of the LDOS on the relative position with respect to the impurity $(\vec{r})$ at low energies. In this range, the physics is dominated by linearly dispersing quasiparticles close to the Dirac points. We find that spatial variations of the LDOS due to the impurity are given by
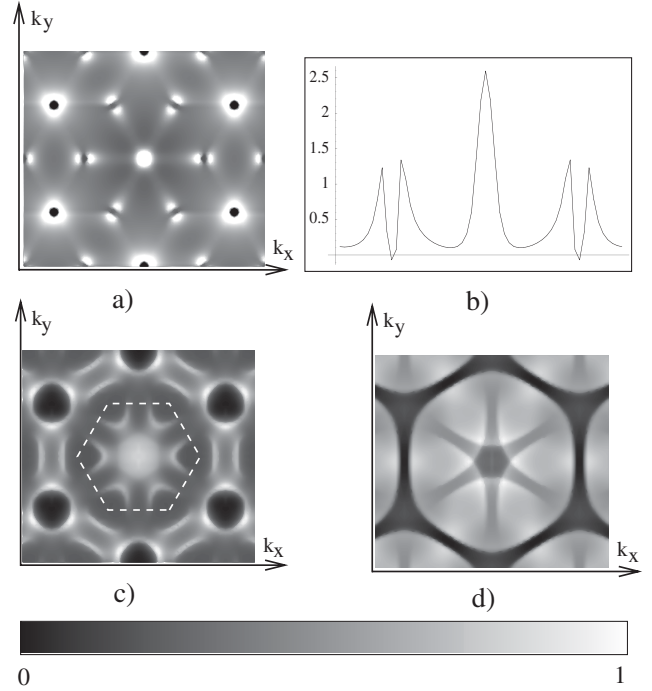

FIG. 1. FTSTS spectra for a monolayer graphene sample with a single delta-function impurity. (a), (c), and (d) correspond to energies $0.15t$, $0.6t$, and $1.2t$ respectively, at $\delta = 0.07t$. The BZ is indicated by dashed lines. The actual lowest (0) and highest (1) values of the FTSTS intensity are different for each energy [$(-1.3, 2.6)$ for $0.15t$, $(-0.8, 5.9)$ for $0.6t$, and $(-6.2, 7.2)$ for $1.2t$ in arbitrary units]. (b) shows a cross section of the FTSTS intensity as a function of k_x for $k_y = 0$, and for energy $0.15t$.

$$\rho(\vec{r}, E) \propto -\text{Im}[\mathcal{G}(-\vec{r}, E)T(E)\mathcal{G}(\vec{r}, E)]$$
$$\approx -\sum_{m,n} \text{Im}[e^{i(\vec{K}_m - \vec{K}_n) \cdot \vec{r}} G_m(-\vec{r}, E)T(E)G_n(\vec{r}, E)], \tag{4}$$

where m, n denote the corresponding Dirac points. Here $T(E)$ is the T matrix, which for a delta-function impurity is given by [9] $T(\omega) = [I - V \int \frac{d^2\vec{k}}{S_{\text{BZ}}} \mathcal{G}(\vec{k}, \omega)]^{-1}V$, where I is the 2×2 identity matrix, and the integration over $\vec{k}$ is performed on the BZ, whose area is $S_{\text{BZ}} = 8\pi^2/3\sqrt{3}$.

Using Eq. (3) and expanding the Hankel functions to leading order in $1/r$, we find that far from the impurity $(\omega r/v \gg 1)$ the corrections to the local density of states due to scattering between the nodes m and n are given by

$$\rho_{mn}(\vec{r}, \omega) \propto \frac{\omega}{r} \text{Im}\{t(\omega)e^{i(\vec{K}_m - \vec{K}_n) \cdot \vec{r} + 2i\omega r/v}i[1 - \phi_m^*(\vec{r})\phi_n(\vec{r})]\}, \tag{5}$$

where $t(\omega)$ is the nonzero element of the T matrix (T_{11}), and we used the fact that $\phi(-\vec{r}) = -\phi(\vec{r})$.

In the case of intranodal scattering ($m = n$) the above expression vanishes and the LDOS is dominated by the next leading correction $\rho_m(\vec{r}, \omega) \propto \sin(2\omega r/v)/r^2$. This is different from what usual wisdom would suggest for a two-

dimensional system ($1/r$ decay) [3,4], and has also been described in Refs. [1,2]. We should note that the two-dimensional FT of $\sin(2\omega r/v)/r^2$ is roughly $\rho_m(q, \omega) \propto \pi\theta(2\omega - qv)/2 + \arcsin(2\omega/qv)[1 - \theta(2\omega - qv)]$. This corresponds to a filled circle of high intensity in the FTSTS spectrum, which is consistent with the results of our numerical analysis for the central region of high intensity.

Nevertheless, for the decay of the Fridel oscillations generated by internodal scattering ($m \neq n$), the leading order behavior is $1/r$. The FT of $\cos(2\omega r/v)/r$ is $\theta(qv - 2\omega)/\sqrt{q^2v^2 - 4\omega^2}$, which translates into *empty* circles of high intensity in the FTSTS spectra, consistent with our numerical analysis. However, since the inverse quasiparticle lifetime δ is finite, there will be some broadening of the resonances and some weight inside the circular contours.

For some of the Fridel oscillations generated by internodal scattering, such as the ones between neighboring node pairs [e.g., (1, 3)], the rotational symmetry is broken: $\phi_1^*(\vec{r})\phi_3(\vec{r}) = e^{-i\pi/3}(x + iy)^2$. However, for next-to-nearest-neighbor node pairs [e.g., (3, 5)], $\phi_3^*(\vec{r})\phi_5(\vec{r}) = e^{-i2\pi/3}$, and the oscillations are rotationally invariant. This is consistent with the results of our numerical analysis: the high-intensity regions centered on sites of the reciprocal lattice are rotationally symmetric, while the high-intensity regions close to the corners of the BZ are not.

We now switch gears and consider the case of a single impurity in bilayer graphene. The bilayer graphene consists of two graphene layers stacked on top of each other such that the atoms in the sublattice A of the first layer occur naturally directly on top of the atoms in the sublattice $\tilde{B}$ of the second layer [10], with a tunneling coupling of t_p. We consider the case of an impurity located on the sublattice A. The case of a single impurity located on a site of a different type, as well as the case of multiple impurities will be presented elsewhere. The resulting FTSTS spectra for the LDOS in the top layer are presented in Fig. 2.

Note that there are similarities and discrepancies between the monolayer and bilayer cases. As in the monolayer case, there are areas of high intensity centered on the corners of the BZ, as well as on the sites of the reciprocal lattice. The main difference at low energy is that the central region of high intensity is an empty circle, and not a full circle (as for the monolayer case). At high energy, we also note a doubling of the number of high-intensity lines corresponding to the doubling of the number of bands.

An analytical study can be performed at low energies starting from the expansion of the Hamiltonian around the Dirac points m. In the sublattice basis $(A, \tilde{B})$ this yields [11]:

$$\mathcal{H}_m^{\text{bilayer}}(\vec{k}) = \begin{pmatrix} 0 & [\tilde{\phi}_m(\vec{k})]^2 \\ [\tilde{\phi}_m^*(\vec{k})]^2 & 0 \end{pmatrix} \tag{6}$$
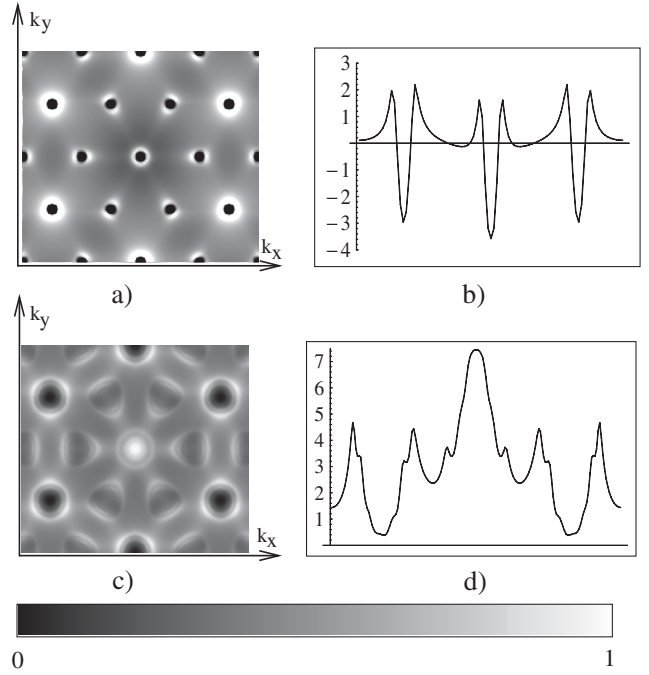

FIG. 2. FTSTS spectra for a bilayer sample. (a) and (c) depict the FTSTS intensity in arbitrary units at energies $0.1t$, $0.4t$, with $t_p = 0.3t$, and $\delta = 0.05t$. The actual lowest (0) and highest (1) values of the FTSTS intensity are $(-6.9, 3.6)$ and $(-6.0, 7.4)$, respectively. (b) and (d) are cross sections at $k_y = 0$ of (a) and (c).

where for simplicity we have set the effective mass of the quadratic spectrum to 1. The corresponding Green's function in real space is given by

$$G_m(\vec{r}, \omega) \propto \begin{pmatrix} H_0^{(1)}(z) & -[\phi_m(\vec{r})]^2 H_2^{(1)}(z) \\ -[\phi_m^*(\vec{r})]^2 H_2^{(1)}(z) & H_0^{(1)}(z) \end{pmatrix} \tag{7}$$

where we denoted $z = r\sqrt{|\omega|}/v$. Starting from Eq. (4), we perform a similar analysis to the case of monolayer graphene. Thus we note that at large distances ($z \gg 1$), as opposed to the monolayer case, the leading ($1/r$) contribution for intranodal scattering is nonvanishing:

$$\rho_m(\vec{r}, \omega) \propto \frac{1}{r\sqrt{|\omega|}} \cos(r\sqrt{|\omega|}/v). \tag{8}$$

This is consistent with the appearance of an empty circular contour at the center of the BZ, as opposed to the filled circle for the monolayer case. The leading contribution to the decay of the oscillations due to internodal scattering is also $1/r$. Note that in the monolayer case the amplitude of the Friedel oscillations corresponding to intranodal scattering is independent of energy, and the amplitude of the Friedel oscillations corresponding to internodal scattering increases as ω^2, while for the bilayer case all oscillations decrease with energy as $1/\sqrt{|\omega|}$.
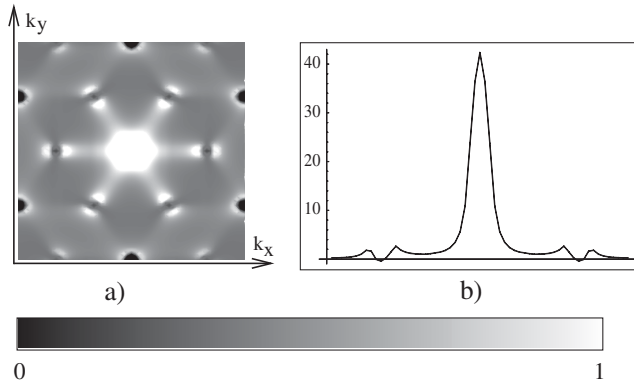
FIG. 3.　FTSTS spectra for a graphene monolayer with a screened-Coulomb impurity at energy $0.2t$, and $\delta = 0.07t$. The lowest and highest values of the intensity are $(-1.7, 42.3)$ in arbitrary units. (b) presents a cross section at $k_y = 0$.

The third system we consider is a monolayer graphene sample with a single screened-Coulomb (charged) impurity. Its impurity potential (in momentum space) has $V_{11} = V_{22} \propto 1/(q + 1/\epsilon_0)$, where $\epsilon_0 \approx 4.5a$ is the screening length [12]. Given the momentum dependence of the impurity, one can no longer use the T-matrix approximation, and must use instead the Born approximation. Our results are plotted in Fig. 3. Note that the intensity of the outer areas of high intensity is very much reduced compared to the intensity of the inner area. This is consistent with the form of the scattering potential, which generates less scattering between quasiparticles located on different nodes than between quasiparticles located on the same node. Similar qualitative differences have also been found between the LDOS oscillations generated by the "mirage" images of Coulomb-type impurities and delta-function impurities in graphene pn junctions [13].

To conclude, we have computed the effect of single-impurity scattering on the Fourier transform of the LDOS, which is measurable experimentally by FTSTS. We have found that the FTSTS spectra in the vicinity of an impurity are a very good tool to distinguish between monolayer and bilayer graphene. In particular, for monolayer graphene, the Friedel oscillations due to intranodal scattering decay as $1/r^2$ and are rotationally invariant. In the FTSTS spectra they correspond to a filled high-intensity circular region at the center of the BZ. On the other hand, the Fridel oscillations due to internodal scattering decay as $1/r$. They lead to different FTSTS features, such as circular contours of high intensity centered around the corners of the BZ and on sites of the reciprocal lattice. Some of these contours display a breaking of rotational invariance. For the bilayer

case both the internodal and the intranodal Fridel oscillations decay as $1/r$.

We have also showed that the FTSTS spectra can be used to distinguish between different types of impurities, for example, between a delta-function impurity and a screened Coulomb scatterer.

Last, but not least, we have noticed that, while the FTSTS spectra in the presence of an impurity can give information on the band structure, they are not fully determined by it, but also contain very important information about the specific form of the Hamiltonian. We believe that this feature is very important, and could be also used in the case of cuprates to understand the physics of high temperature superconductivity.

[1]　V. V. Cheianov and V. I. Fal'ko, Phys. Rev. Lett. **97**, 226801 (2006).

[2]　E. Mariani *et al.*, Phys. Rev. B **76**, 165402 (2007).

[3]　C. Bena and S. Kivelson, Phys. Rev. B **72**, 125432 (2005).

[4]　S. A. Kivelson *et al.*, Rev. Mod. Phys. **75**, 1201 (2003).

[5]　T. O. Wehling *et al.*, Phys. Rev. B **75**, 125425 (2007); N. M. Peres *et al.*, Europhys. Lett. **80**, 67007 (2007); N. M. Peres, F. Guinea, and A. H. Castro Neto, Phys. Rev. B **73**, 125411 (2006); Phys. Rev. B **73**, 125411 (2006); M. A. H. Vozmediano *et al.*, Phys. Rev. B **72**, 155121 (2005); T. Ando, J. Phys. Soc. Jpn. **75**, 074716 (2006); Y. G. Pogorelov, arXiv:condmat/0603327; Y. V. Skrypnyk and V. Loktev, Phys. Rev. B **73**, 241402(R) (2006); Phys. Rev. B **75**, 245401 (2007); M. I. Katsnelson and A. K. Geim, Phil. Trans. R. Soc. A **366**, 195 (2008).

[6]　P. Mallet *et al.*, Phys. Rev. B **76**, 041403(R) (2007); G. M. Rutter *et al.*, Science **317**, 219 (2007).

[7]　F. Vonau *et al.*, Phys. Rev. Lett. **95**, 176803 (2005); F. Vonau *et al.*, Phys. Rev. B **69**, 081305 (2004); E. Dupont-Ferrier *et al.*, Europhys. Lett. **72**, 430 (2005).

[8]　See, e.g., K. McElroy *et al.*, Science **309**, 1048 (2005); M. Vershinin *et al.*, Science **303**, 1995 (2004); A. Fang *et al.*, Phys. Rev. B **70**, 214514 (2004).

[9]　J. M. Byers, M. E. Flatté, and D. J. Scalapino, Phys. Rev. Lett. **71**, 3363 (1993); M. I. Salkola, A. V. Balatsky, and D. J. Scalapino, Phys. Rev. Lett. **77**, 1841 (1996); W. Ziegler *et al.*, Phys. Rev. B **53**, 8704 (1996).

[10]　P. Van Mieghem, Rev. Mod. Phys. **64**, 755 (1992); E. McCann, Phys. Rev. B **74**, 161403 (2006).

[11]　E. McCann and V. I. Fal'ko, Phys. Rev. Lett. **96**, 086805 (2006); J. Nilsson *et al.*, Phys. Rev. B **73**, 214418 (2006).

[12]　M. I. Katsnelson, Phys. Rev. B **76**, 073411 (2007).

[13]　V. Cheianov *et al.*, Science **315**, 1252 (2007).